Green synthesis, characterization, and biomedical applications of Iron nanoparticles synthesized from the alcoholic extract of the aerial part of Micromeria biflora (Buch. Ham. ex D.Don) Benth

Abdur Rauf
University of Swabi
Muhammad Ibrahim
University of Swabi
Zubair Ahmad
University of Swabi
Naveed Muhammad
University Mardan
Yahya S. Al-Awthan
University of Tabuk
Omar S. Bahattab
University of Tabuk
Saeed Hameed Rami
Umm Al-Qura University
Saud Bawazeer
Umm Al-Qura University
Imran Ullah
Rekha Thiruvengadam
Sejong University
Muthu Thiruvengadam
muthu@konkuk.ac.kr

Konkuk University

Research Article

Keywords: Green synthesis, Iron NPs, Micromeria biflora, Biological activities, Characterizations

Posted Date: April 5th, 2024

DOI: https://doi.org/10.21203/rs.3.rs-4184891/v1

Additional Declarations: No competing interests reported.

Abstract

This study explored the synthesis and characterization of iron nanoparticles (NPs) using *Micromeria biflora* extract. The rapid reduction of iron ions, evidenced by a distinct color change, signifies an efficient interaction, leading to successful NPs formation. UV-visible spectroscopy confirmed the synthesis, revealing an absorption peak at 295 nm that intensified over time. Fourier Transform Infrared (FTIR) spectroscopy demonstrates phytochemical involvement. Field-Emission Scanning Electron Microscopy (FESEM) images displayed cuboctahedron-shaped NPs with various facet formations, which are crucial for diverse applications. DISCUS package was used to simulate the shape and decorate the surface with organic molecules obtained from the extract. Energy Dispersive X-ray Spectroscopy (EDS) was used to confirm the elemental composition. Additionally, potential applications, including enzyme effects and sedative and anti-inflammatory properties, were explored. The extract and NP showed anticancer effects against MDR2780AD cell lines, with IC_{50} values of 1.99 and 0.91 respectively. The tested Iron NPs showed 92.22, 76.22, and 88.23% inhibitory effects against urease, CA-II, and XO, respectively. The maximum percentage analgesic effects of the extract (100 mg/kg) and NPs (10 mg/kg) were 65 and 82, respectively. Maximum anti-inflammatory effect was observed at the third hour of treatment. The anti-inflammatory effect of NP (90%) was superior to that of the extract (60%).

1. Introduction

The fields of medicine and healthcare have seen a rise in the significance of nanotechnology in recent decades [1]. Thus, different sector specialists are adapting green synthesis procedures that can produce environmentally friendly nanoparticles (NPs) [2]. As a result, emphasis is being placed on developing technologies that are both environmentally benign and nutrient-rich. Nanoparticles possess a large surface area and are characterized by their small size and high reactivity [3]. Thus, the application of green technology is currently more widespread than ever before. The primary goal of nanotechnology is to create nanoscale particles that are more efficient and beneficial for human welfare [4]. These particles have flexible forms, regulated chemical compositions, and are small in size. It is possible to create pure nanoparticles with known properties using various physical and chemical methods [5]. Green synthesis, also called biological synthesis, is a low-cost, environmentally friendly method for producing large quantities of nanoparticles without the use of hazardous chemicals, high temperatures, or high pressures [6]. This allows for improvements in the synthesis of nanoparticles. Green synthesis uses biological sources, including plant extracts and microorganisms, to reduce and stabilize metal ions, resulting in the formation of nanoparticles. This method's benefits include biocompatibility, environmental sustainability, and scalability for large-scale production [4, 7]. Owing to their exceptional qualities and numerous possible uses, iron NPs (FeNPs) have drawn considerable interest. FeNPs have a high surface-to-volume ratio owing to their nanoscale size, which creates more active areas for biological interactions, catalysis, and adsorption. Because iron is abundant and biocompatible, Iron NPs are attractive for biomedical applications such as imaging and drug delivery [8, 9].

For thousands of years, tribes worldwide have used herbal remedies as medicine. Plants have been a frequent source of therapeutic therapy since the beginning of time and up until the end of the nineteenth century [10, 11]. Despite saving lives in some domains, mass-produced chemical medications have swept aside this large corpus of knowledge during the 20th century and have not proven to be an all-encompassing cure that experts have hoped for. Because the majority of plants are now widely used for culinary and therapeutic purposes [12], researchers are interested in the chemistry of medicinal plants [13–17]. The genus *Micromeria* (Lamiaceae family) is useful in treating colds, wounds, headaches, skin infections in cattle, and cardiac problems. Leaf powder combined with oil is used to treat fungal infections and ulcers [18, 19]. This genus includes over 100 species, which are extensively dispersed worldwide. *Micromeria biflora*, *M. capitellata* and *M. biflora* var. *hispida* are the only three species known to exist in the Indian Himalayan region. Several essential oils have been shown to have anti-inflammatory properties [20]. Owing to the rich phytochemical profile of *M. biflora* and the versatility of Iron NPs, we used the extract of *M. biflora* as a reducing and stabilizing agent for the synthesis of Iron NPs in an ecofriendly manner for enhanced biological application.

2. Material and Experimental

2.1 Collection of plant and extractions

Micromeria biflora was collected in the Dir District, Khyber Pakhtunkhwa, Pakistan. After cleaning and washing with deionized water, they were left to dry in the shade for two weeks. The material was then broken into small pieces with a knife that had been cleaned in methanol, crushed using a mortar and pestle, added to 20 mL of sterile deionized water, and heated at a moderate temperature for two–three minutes. The extract was then filtered through a Whatman No. 1 filter paper. The filtrate was collected in a sterile dry conical flask and kept at room temperature using a standard sterile filtration procedure.

2.2 Synthesis of Iron NPs

To fabricate Iron NPs, precursor and reducing agent were mixed in a 10:1 ratio in a sterile, clean flask. For the reduction of Fe ions, 10 mL of freshly prepared 0.001 M aqueous $FeCl_3$ solution and 10 mL of filtered plant extract were combined, and they were continuously agitated at 50°C to 60°C. The quick transition from light green to black demonstrated the efficiency of the nanoparticle manufacturing process. The general overview is depicted in Fig. 1.

2.3 Instrumental Characterizations

Several characterization techniques were employed to closely evaluate the size, shape, and elemental composition of the synthesized iron oxide NPs. UV spectroscopy was performed using a UV-Vis spectrophotometer (Model-UV2601) to obtain the absorbance spectra of the Iron NPs. The functional groups responsible for the stabilization and reduction of metal ions in the plant extract were identified by FTIR (Model FTIR-990) using the KBr pellet method. The form and texture of the iron-oxide NPs were

examined using SEM. EDS analysis was also carried out to ascertain the elemental composition of the iron oxide NPs.

2.4 Simulation of Iron NPs

Iron NPs derived from the alcoholic extract of *M. biflora* were simulated using the DISCUS package to investigate the interaction of the active sites on the surface with the extract. The simulation starts by reading the asymmetric unit cell of NP, which belongs to a cubic crystal system with lattice parameters $a = b = c$and $\alpha = \beta = \gamma = 90^{\circ}$. The unit cells were extended in the a, b, and c directions and cut to the appropriate size. Salicylalazine, an organic molecule known for its potential biomedical applications, is a promising compound isolated from *M. biflora* extracts. The surface of the simulated NPs was decorated with organic molecules.

2.5 *In vitro* Biological screening

2.5.1 Urease activity

The inhibition of urease activity by Iron NPs synthesized from *M. biflora* extract was investigated. The experimental procedure involved incubating 25 µL of urease enzyme, 55 µL of buffer solution containing 100 mM urea, and 5 µL of synthesized Iron NPs at 30°C for 15 min in 96-well plates. Urease activity was assessed by monitoring ammonia production using the indophenol method. A mixture comprising 45 µL phenol reagent (1% w/v phenol and 0.005% w/v sodium nitroprusside) and 70 µL alkali reagent (0.5% w/v NaOH and 0.1% active chloride NaOCl) was added to each well. Subsequently, absorbance at 630 nm was measured after 50 min using a microplate reader. The assay was conducted in triplicate, with a final volume of 200 µL in each well. Thiourea was employed as a reference control [21]. The percentage of inhibition of urease activity was calculated using the following formula:

$$Percenteffect = 100 - \frac{\mathrm{ODtestwell}}{\mathrm{ODcontrol}} X100$$

2.5.2 Carbonic anhydrase II enzyme activity

We determined whether the synthesized Iron NPs had an inhibiting effect on the activity of carbonic anhydrase II. The amount of hydrated carbon dioxide was measured using a pH indicator. The test sample (Iron NPs), enzyme Carbonic Anhydrase II, and substrate made up the reaction mixture. The reaction was carried out at pH and temperature where the enzyme activity peaked. The change in pH following incubation was determined using a pH indicator. The percentage inhibition of Carbonic Anhydrase II enzyme activity by the NPs was computed by comparing the pH change in the presence and absence of iron oxide NPs. Three replicates of each experiment were performed [22].

2.5.3 Xanthine oxidase activity

Xanthine oxidase activity was measured using the hydroxylation reaction of xanthine as the substrate, leading to the formation of colorless uric acid as the end product. The absorbance of uric acid was

measured at 296 nm. The reaction mixture consisted of the test sample (Iron NPs), phosphate buffer, and xanthine oxidase. A 1 mmol/L test sample solution was prepared and 10 µL of this solution was dissolved in dimethyl sulfoxide (DMSO). Additionally, 0.003 units of xanthine oxidase enzyme was dissolved in 20 µL of phosphate buffer, and 20 µL of xanthine (0.1 $mmol.L^{-1}$) served as the substrate. After addition of xanthine oxidase, the mixture was incubated for 10 min at room temperature. Subsequently, the mixture was analyzed in the UV region (λmax = 295 nm). Following this, the substrate was added, and absorbance readings were recorded at 1-minute intervals for 15 min using a microplate reader. The percentage inhibition of the Iron NPs was then calculated. Absorbance (A) was determined using the formula A = aλ × b × c, where aλ represents the absorptivity coefficient at a specific wavelength, b denotes the path length, and c is the concentration of the analyte. Allopurinol was used as a positive control, and the inhibitory activity of the test samples was compared with that of the standard. The experiment was performed in triplicate to ensure reliability and reproducibility of the results [23].

2.5.4 Anticancer effect

The cytotoxicity of the synthesized IOPNs assessed using the MTT assay, as described in previous studies conducted by Burhan *et al*. (2022) and Muhammad *et al*. (2012) [24, 25]. The A498 cell line, derived from renal tissue; the HepG2 cell line, derived from human hepatoma; the NCI-H226 cell line, derived from non-small cell lung tissue; and the 2780AD cell line, derived from multidrug-resistant human ovarian cancer, maintained in artificial culture media.

2.6 *In vivo* analysis

2.6.1 Analgesic

The acetic acid-induced writhing test was used to assess the analgesic effects. The animals were classified as negative control (10 ml/kg DW), positive control (5 mg/kg diclofenac sodium), and the tested groups were treated with extract (25, 50, and 100 mg/kg) and Iron NPs (2.5, 5, and 10 mg/kg). Thirty minutes after administration, the animals were treated with acetic acid (1%, IP). After 10 min of acetic acid administration, the abdominal contractions were counted for 10 min, and the percent activity was calculated using a published formula [25].

2.6.2 Sedative screening

An open field test was used to evaluate the selected samples. In this study, animals were classified as negative control (10 mL/kg, DW), positive control (diazepam 0.25 mg), and the tested groups were treated with extract (25, 50, and 100 mg/kg) and Iron NPs (2.5, 5, and 10 mg/kg). After (30 min) the animals were placed individually at the center of a special box (the box was made of wood, and the bottom was marked with a black marker of 19 lines with equal spaces). The number of crossed lines was counted for each mouse for 10 minutes. greater the number of lines crossed reflects a lack of sedative effect, and vice versa [26].

2.6.3 Anti-inflammatory activity

The anti-inflammatory effects of the samples were quantified using a plethysmometer. Animals were classified and treated as in the acetic acid-induced writhing model. After 30 min of administration of DW, diclofenac sodium, diclofenac extract, and Iron NPs. The paw of each animal was treated with carrageenan (0.05 ml) to induce edema (inflammation). Animal paw edema was measured at 0 h and then repeatedly at 1, 2, 3, 4 and 5th h. after completion of observations, the percent effect use was calculated [25].

3. Results and Discussion

3.1 Iron NPs synthesis

The rapid reduction of iron ions by the *M. biflora* extract was readily apparent during iron oxide nanoparticle synthesis. Starting from a pale-yellow solution indicative of free iron ions, the reaction mixture underwent a swift color change to deep brown within the first few minutes. This rapid shift suggests an efficient interaction between the reducing and stabilizing components of the extract and iron ions, leading to the formation of Iron NPs. The characteristic deep brown coloration confirmed the successful synthesis [27].

3.2 UV-Vis. Spectroscopy

UV-visible spectroscopy was employed to confirm the formation of Iron NPs. The spectrum displays a distinct absorption peak at 295 nm (Fig. 2), which is characteristic of Iron NPs. This peak, attributed to surface plasmon resonance (SPR), intensified over time, indicating the gradual formation and growth of the nanoparticles within the reaction mixture. The increasing intensity aligns with the observed color change, reinforcing the successful synthesis of the nanoparticles [28].

3.3 FTIR

Fourier Transform Infrared (FTIR) spectroscopy revealed peaks in the *M. biflora* extract at 3300 cm^{-1} (O-H stretching vibrations), 2200 cm^{-1} (C ≡ C triple bonds), and 1700 cm^{-1} (C = O stretching vibrations). Similar peaks in the FTIR spectrum of plant-mediated Iron NPs (Iron NPs) indicate the involvement of phytochemicals in reducing and stabilizing metal ions, facilitating successful nanoparticle formation. Our results align with studies emphasizing the potential of plant extracts in nanoparticle synthesis. The active involvement of phytochemicals in reducing and stabilizing metal ions, as indicated by FTIR peaks, is consistent with the broader literature in green synthesis methods [29, 30]. The FTIR spectra are shown in the inset of Fig. 3.

3.3 SEM and EDS

The morphology and elemental composition of the Iron NPs were examined using Field-Emission Scanning Electron Microscopy (FESEM) and Energy Dispersive X-ray Spectroscopy (EDS). Figure 4 presents FESEM images at both high and low resolutions, highlighting the distinct cuboctahedron shape

and size distribution of the nanoparticles. At high resolution, individual nanoparticles exhibit a well-defined cuboctahedral morphology, a common feature of cubic crystal systems, making them ideal for various applications. The low-resolution image provides an overview, indicating a remarkably consistent size distribution across the majority of nanoparticles. EDS analysis revealed the elemental composition, showing percentages by mass of 25.80% carbon, 2.45% nitrogen, 12.21% oxygen, and 0.11% Fe (Fig. 5). These results confirmed the presence of Iron NPs.

3.4 Salicylalazine Decorated NPs

FESEM images revealed the cuboctahedral morphology of the Iron NPs. Salicylalazine was extracted from *M. biflora* and used as a ligand molecule. Convergence of nanotechnology and biomedical science. The decoration of Iron NPs with Salicylalazine led to dual functionality. First, salicylalazine acts as a modulator of NP growth kinetics, precisely controlling growth dimensions to preserve the desired cuboctahedral morphology and enhance NP stability, thereby reducing the tendency toward aggregation or Oswald ripening. Decoration typically involves sophisticated surface functionalization techniques and capitalizes on the chemical properties of both salicylalazine and iron NPs. Various functional groups, including hydroxyl and amine groups, in salicylalazine provide anchoring points for attachment. They are attached through coordination bonds, hydrogen bonding, van der Waals forces, or electrostatic interactions. The simulation clearly indicated ligand exchange reactions and direct incorporation during synthesis [31]. This complex process involves a combination of chemical reactions and surface modification techniques, yielding functionalized Fe NPs with improved stability and promising biological potential. The simulated and decorated NPs are shown in Fig. 6.

4. Anticancer effect

The anticancer effects of the crude extract and Iron NPs on different cell lines are presented in Table 1. The maximum anticancer effect interim of IC50 was observed against MDR2780AD by the extract and Iron NPs with IC50 values of 1.99 and 0.91 respectively. A variable degree of anticancer effect was also noted for HepG2, A498, and NCI-H226 cell lines. Similarly, anticancer activity of iron nanoparticles using *Punica granatum* aqueous extract [32]. The anticancer activities of the tested samples were also assessed against the reference compound paclitaxel. While Paclitaxel demonstrated potent anticancer effects across all cell lines with notably low IC50 values, the crude extract and Iron NPs exhibited competitive efficacy, particularly against the MDR2780AD cell line. These findings suggest that both crude extract and Iron NPs possess promising anticancer properties. Additionally, the observed efficacy against multidrug-resistant cancer cell lines highlights the significance of these compounds in overcoming drug resistance, which remains a major obstacle in cancer treatment. Further studies are warranted to elucidate the underlying mechanisms and optimize the therapeutic potential of these compounds for clinical translation.

Table 1
Anticancer Activities

Compounds	IC_{50}			
	HepG2	A498	NCI-H226	MDR 2780AD
Extract	170.98 ± 0.43	160.99 ± 0.77	133.65 ± 1.45	1.99 ± 0.45
Iron NPs	30.12 ± 0.34	178.09 ± 0.87	118.55 ± 0.43	0.91 ± 0.24
Paclitaxel	7.99 ± 0.67	97.11 ± 0.33	62.00 ± 0.23	0.21 ± 0.04

3.2 Effect on Urease

The effects of the extract and Iron NPs on urease activity are presented in Table 2. The tested Iron NPs resulted in a 92.22% inhibitory effect compared with the positive control drugs (97%). The effect of the tested extracts was not statistically significant (41%).

Table 2
Urease effects

Sample	Concentration	% inhibition	IC_{50}
Extract	0.25 µg/ml	41.07	-
Iron NPs	0.25 µg/ml	92.22	7.66 ± 1.00
Thiourea	0.25 mM/ml	97.97	0.21 ± 0.43

3.3 Effect on CA-II

The effects of the extract and Iron NPs as inhibitors is shown in Table 3. The effect of Iron NP was greater than that of the crude extract. The Percent effect of both tested samples was 48.27 and 76.22%, respectively.

Table 3
Carbonic anhydrase II enzyme effects

Sample	Concentration	% inhibition	IC_{50}
Extract	0.25 µg/ml	48.27	-
Iron NPs	0.25 µg/ml	76.22	27.01
Acetazolamide	0.25 mM/ml	81.01	15.11 ± 1.21

3.4 Effect on XO

CA-II was significantly antagonized by Iron NPs (88.23%) compared to allopurinol (96.22%). The crude extract antagonized XO with a non-significant percentage value (Table 4).

Table 4
Xanthine oxidase effects

Sample	Concentration	% inhibition	IC_{50}
Extract	0.25 µg/ml	39.09	-
Iron NPs	0.25 µg/ml	88.23	24.19 ± 1.20
Allopurinol	0.25 mM/ml	96.22	0.72 ± 0.80

3.5 Analgesic effect

The analgesic effects of acetic acid on writhing are shown in Table 5. A dose-dependent effect was observed in both tested samples. The maximum percent effects of the extract (100 mg/kg) and NPs (10 mg/kg) were 65 and 82%, respectively.

Table 5
Analgesic effects

Treatment	Dose (mg/kg)	Percent effect
Saline	10 ml/kg	-
Extract	25	49.87 ± 1.87
	50	61.66 ± 1.92
	100	65.43 ± 1.66
Iron NPs	2.5	59.02 ± 1.65
	5	71.21 ± 1.23
	10	82.89 ± 1.66
Diclofenac sodium	5	85.02 ± 0.32

3.6 Sedative effect

The dose-dependent sedative effects of the extract and NP are shown in Table 6. A significant ($P < 0.001$) effect was observed for the extracts and NP. The sedative effect of NP was greater than that of extract alone. The positive control drug showed a highly significant sedative effect compared with the other tested samples.

Table 6
Sedative screening effects

Treatment	Dose (mg/kg)	Number of lines crossed in 10 minutes
Saline	10 ml/kg	134.06 ± 0.97
Extract	25	66.23 ± 1.88*
	50	60.7 ± 1.98**
	100	52.30 ± 1.60***
Iron NPs	2.5	36.66 ± 1.30***
	5	28.76 ± 1.09***
	10	18.66 ± 1.04***
Diazepam	0.25	1.12 ± 1.36***

3.7 Anti-inflammatory effects

The anti-inflammatory effects of the tested samples are shown in Fig. 7. The maximum attenuation of paw edema was observed at the third hour of treatment. The anti-inflammatory effect of NP (90%) was superior to that of the extract (60%). This antiedematous effect was maintained until the end of the experiment.

4. Conclusion

This study successfully demonstrated the efficient and eco-friendly synthesis of Iron NPs (Iron NPs) using *M. biflora* extract. The observed color change and confirmed synthesis using various techniques underscores the potential of this green synthesis approach. The crucial aspect of this research was the anchoring of salicylalazine to the surface of the NPs. This enhances the stability and therapeutic potential of the NPs. The selected samples had significant anticancer, analgesic, sedative, and anti-inflammatory properties. These biological effects support the use of folklore in the treatment of headaches, sinusitis, inflammation, and other ailments.

Declarations

Acknowledgements The authors thank the Department of Chemistry University of Swabi for providing facility to do this work.

Funding Not Applicable

Data availability Data will be made available on request.

Conflict of interests The authors declare that they have no known competing fnancial interests or personal relationships that could have appeared to infuence the work reported in this paper.

Ethical approval Not applicable.

Author Contribution

A.R., M.I., Z.A., M.T and N.M: writing – original draft, writing – review and editing, visualization, methodology, experiment. Y.S.A., O.S.B., S.H.R., S.B., I.U., and R.T writing – review and editing, formal analysis, visualization, resources.

References

1. Saxena, S.K., et al., *Current advances in nanotechnology and medicine.* NanoBioMedicine, 2020: p. 3-16.
2. Gour, A. and N.K. Jain, *Advances in green synthesis of nanoparticles.* Artificial cells, nanomedicine, and biotechnology, 2019. **47**(1): p. 844-851.
3. Khan, I., K. Saeed, and I. Khan, *Nanoparticles: Properties, applications and toxicities.* Arabian journal of chemistry, 2019. **12**(7): p. 908-931.
4. Ying, S., et al., *Green synthesis of nanoparticles: Current developments and limitations.* Environmental Technology & Innovation, 2022. **26**: p. 102336.
5. Sajid, M. and J. Płotka-Wasylka, *Nanoparticles: Synthesis, characteristics, and applications in analytical and other sciences.* Microchemical Journal, 2020. **154**: p. 104623.
6. Salem, S.S. and A. Fouda, *Green synthesis of metallic nanoparticles and their prospective biotechnological applications: an overview.* Biological trace element research, 2021. **199**: p. 344-370.
7. Rahman, H., et al., *Green Synthesis of Silver Nanoparticles Using Rhazya stricta Decne Extracts and Their Anti-Microbial and Anti-Oxidant Activities.* Crystals, 2023. **13**(3): p. 398.
8. Rukhsar, M., et al., *An overview of iron oxide (Fe3O4) nanoparticles: From synthetic strategies, characterization to antibacterial and anticancer applications.* Crystals, 2022. **12**(12): p. 1809.
9. Aljohny, B.O., et al., *Cellulose acetate composite films fabricated with zero-valent iron nanoparticles and its use in the degradation of persistent organic pollutants.* Applied Organometallic Chemistry, 2020. **34**(11): p. e5892.
10. Hafeez, N., *Phytochemical and Biological Studies of Cucurbitaceae: A Mini-Review.* Phytopharmacology Research Journal, 2024. **3**(1): p. 13-23.
11. Khan, I.A., S. Khan, and H. Bilal, *Qualitative Phytochemical Screening of Buddleja crispa (roots and stem).* Phytopharmacology Research Journal, 2024. **3**(1): p. 1-07.

12. shahab Khan, M., et al., *In vitro screening of Cichorium intybus, a local medicinal plant for antimicrobial activities.* Phytopharmacology Research Journal, 2022. **1**(2): p. 1-10.
13. Petrovska, B.B., *Historical review of medicinal plants' usage.* Pharmacognosy reviews, 2012. **6**(11): p. 1.
14. Rauf, A., et al., *Antiproliferative Activity of Lignans from Olea ferruginea: In Vitro Evidence Supported by Docking Studies.* Frontiers in Bioscience-Landmark, 2023. **28**(9): p. 216.
15. Ahmad, Z., B. Muhammad, and N. Khan, *Pharmacokinetics of Natural Compounds: Unlocking the Therapeutic Potential.* Phytopharmacology Research Journal, 2023. **2**(2): p. 22-25.
16. Rauf, A., et al., *Density functional theory, molecular docking, In vitro and In vivo anti-inflammatory investigation of lapachol isolated from Fernandoa adenophylla.* Heliyon, 2023. **9**(12).
17. Syed, A.L., et al., *GC-MS analysis, antimicrobial, antioxidant, phytochemical, and phytotoxic activities of Elaeagnus angustifolia L. using different extracts.* Phytopharmacology Research Journal, 2023. **2**(3): p. 1-12.
18. Pedro, L.G., et al., *Composition of the essential oil of Micromeria varia Benth. ssp. thymoides (Sol. ex Lowe) Perez var. thymoides, an endemic species of the Madeira archipelago.* Flavour and fragrance journal, 1995. **10**(3): p. 199-202.
19. Aljohani, A.S., et al., *In Vivo and In Vitro Biological Evaluation and Molecular Docking Studies of Compounds Isolated from Micromeria biflora (Buch. Ham. ex D. Don) Benth.* Molecules, 2022. **27**(11): p. 3377.
20. Mahesh, C., et al., *Essential oil composition and pharmacological activities of Micromeria biflora (Buch.-Ham. Ex D. Don) Benth. collected from Uttarakhand region of India.* Journal of Medicinal Plants Research, 2013. **4**(35): p. 2538-2544.
21. Khan, R., et al., *Comparative urease enzyme inhibition profile of leaves and stems of Rumex nervosus vahl.* Natural product research, 2014. **28**(24): p. 2355-2357.
22. Bawazeer, S., et al., *Antioxidant and Enzyme inhibitory activities of extracts and phytochemicals isolated from Pistacia integerrima.* Journal of Medicinal and Spice Plants, 2019. **23**(2): p. 55-58.
23. Alam, M., et al., *In vitro and in silico xanthine oxidase inhibitory potential of Benzofuran isolated from Viburnum grandiflorum Wall. Ex DC.* South African Journal of Botany, 2021. **143**: p. 359-362.
24. Burhan, A., et al., *Anticancer and Cytotoxic Potentials of Vernonia amygdalina Delile on WiDr Cell Lines.* Phytopharmacology Research Journal, 2022. **1**(1): p. 1-7.
25. Muhammad, N., M. Saeed, and H. Khan, *Antipyretic, analgesic and anti-inflammatory activity of Viola betonicifolia whole plant.* BMC complementary and alternative medicine, 2012. **12**: p. 1-8.
26. Muhammad, N., et al., *Evaluation of n-hexane extract of Viola betonicifolia for its neuropharmacological properties.* Journal of Natural Medicines, 2013. **67**: p. 1-8.
27. Beheshtkhoo, N., et al., *Green synthesis of iron oxide nanoparticles by aqueous leaf extract of Daphne mezereum as a novel dye removing material.* Applied Physics A, 2018. **124**: p. 1-7.

28. Ebrahiminezhad, A., et al., *Plant-mediated synthesis and applications of iron nanoparticles.* Molecular biotechnology, 2018. **60**: p. 154-168.
29. Ullah, I., et al., *Peganum harmala L. extract-based Gold (Au) and Silver (Ag) nanoparticles (NPs): Green synthesis, characterization, and assessment of antibacterial and antifungal properties.* Food Science & Nutrition, 2024.
30. Khan, S., et al., *Green synthesis of silver and gold nanoparticles in Callistemon viminalis extracts and their antimicrobial activities.* Bioprocess and Biosystems Engineering, 2024: p. 1-15.
31. Warner, M.G., S.M. Reed, and J.E. Hutchison, *Small, water-soluble, ligand-stabilized gold nanoparticles synthesized by interfacial ligand exchange reactions.* Chemistry of materials, 2000. **12**(11): p. 3316-3320.
32. Liu, J., Liu, G., Li, J., Li, X., Zhou, H., Qiu, C., Almasi, M. (2024). Green formulation of iron nanoparticles by plant extract induces apoptosis via P53 and STAT3 signaling pathways in prostate cancer cells. Inorganic Chemistry Communications, 162, 112164.

Figures

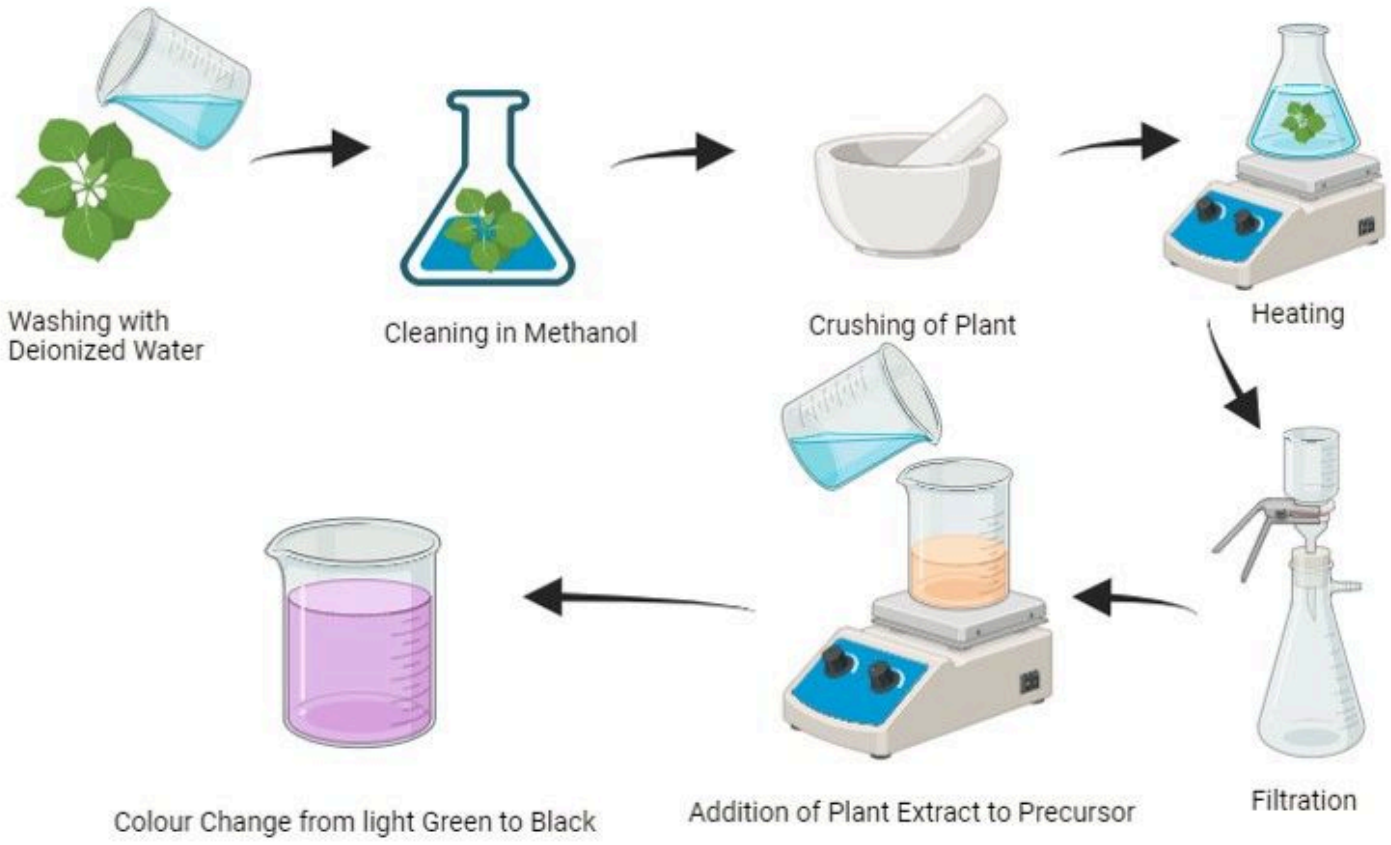

Figure 1

Synthesis Steps of Iron NP

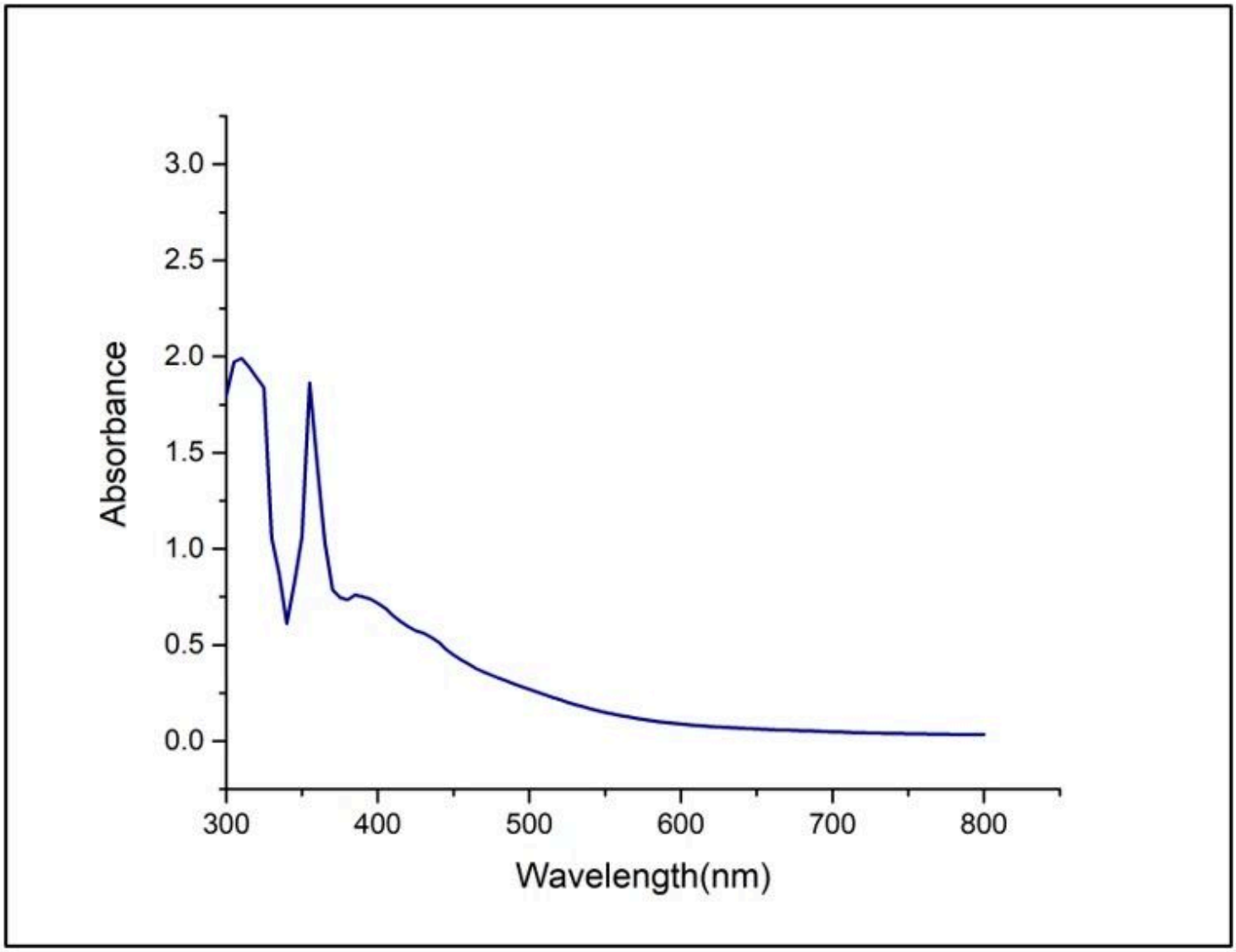

Figure 2

UV-Vis. Spectrum of Iron NPs.

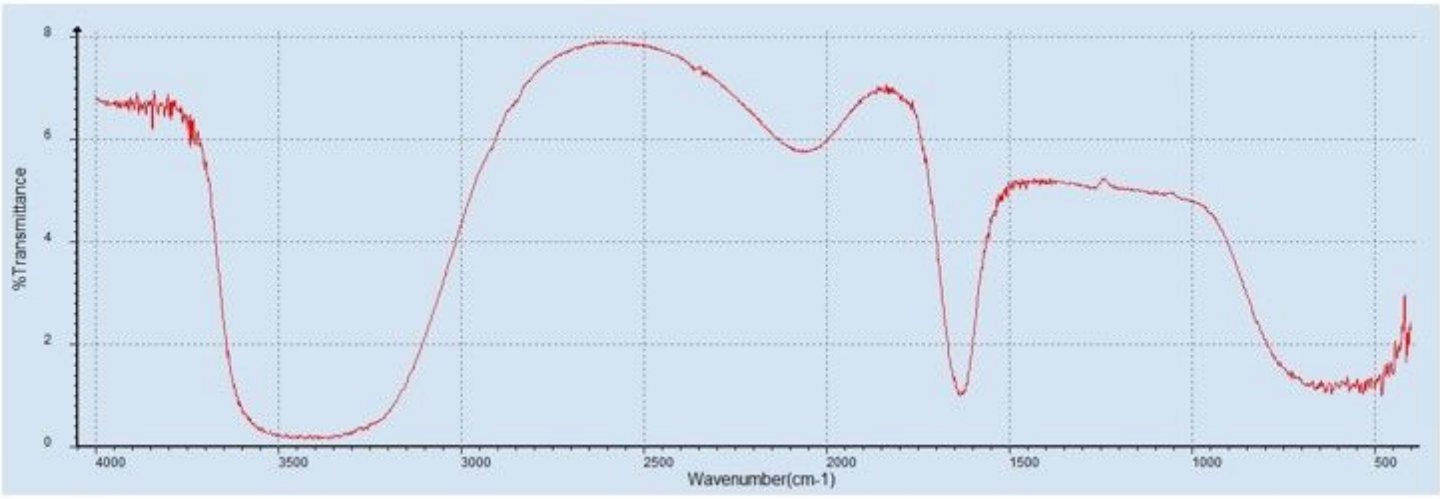

Figure 3

FTIR Spectra of Iron NPs Synthesized from *Micromeria biflora* extract.

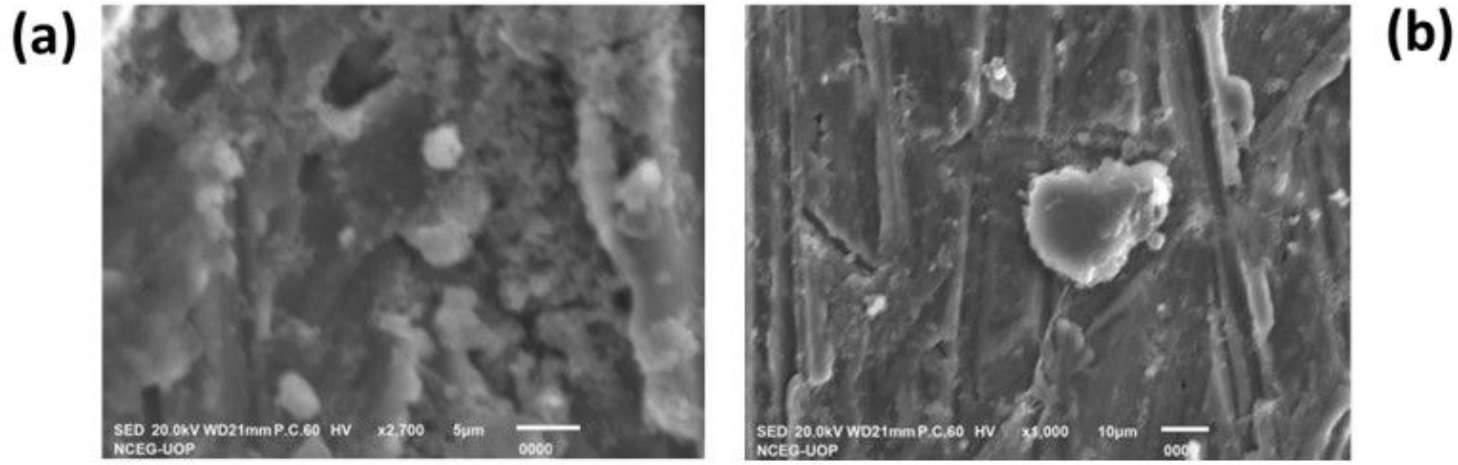

Figure 4

High resolution (a) and low resolution FESEM images of Iron NPs.

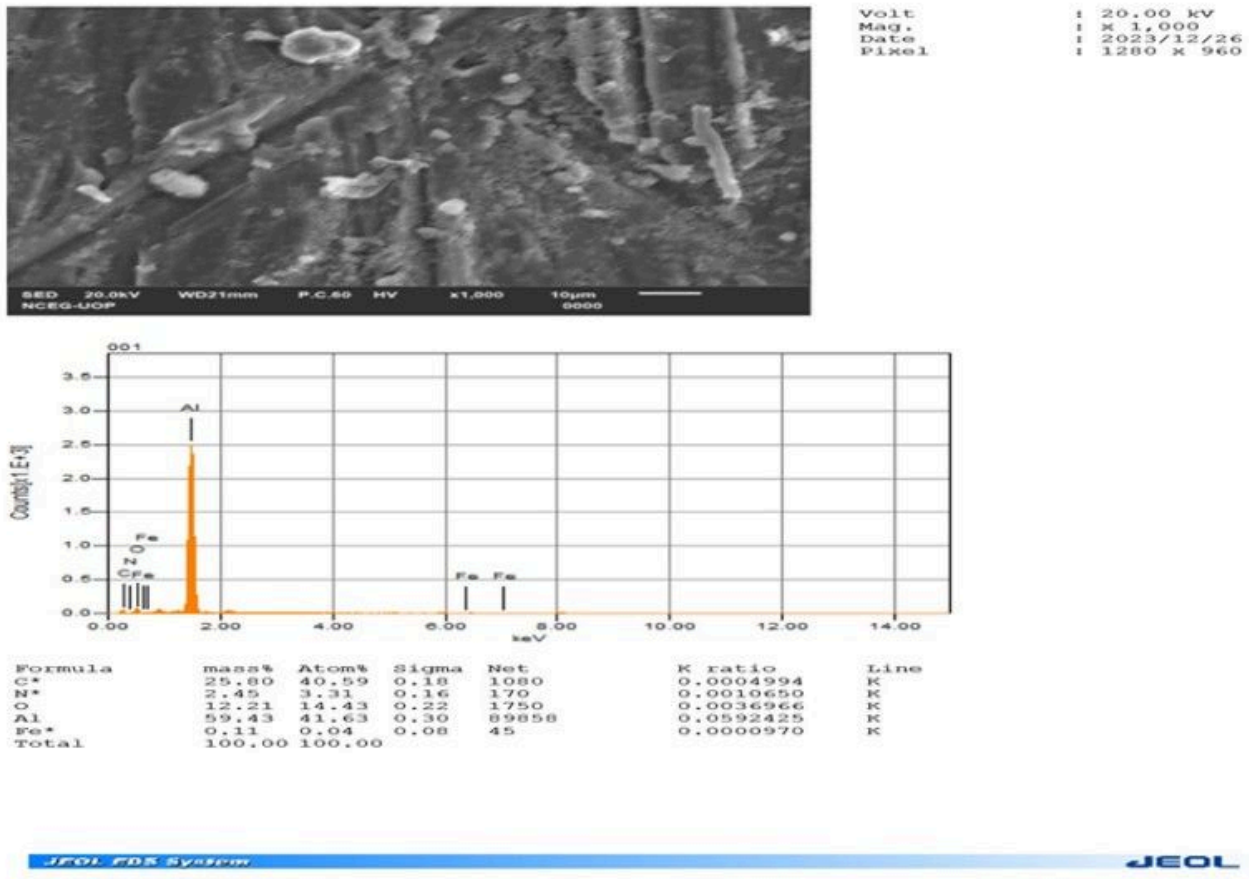

Figure 5

EDS results of synthesized Iron NPs

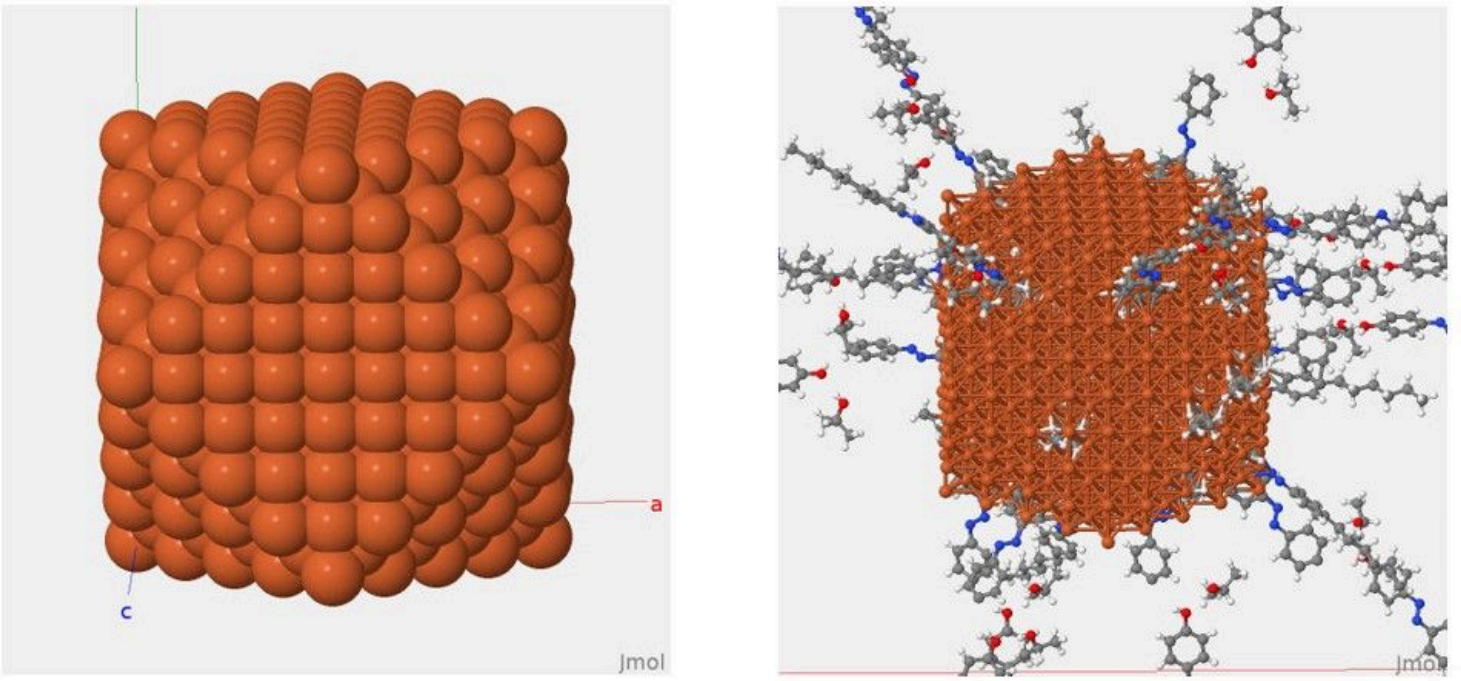

Figure 6

Simulated Iron NPs and Salicylalazine Attachment.

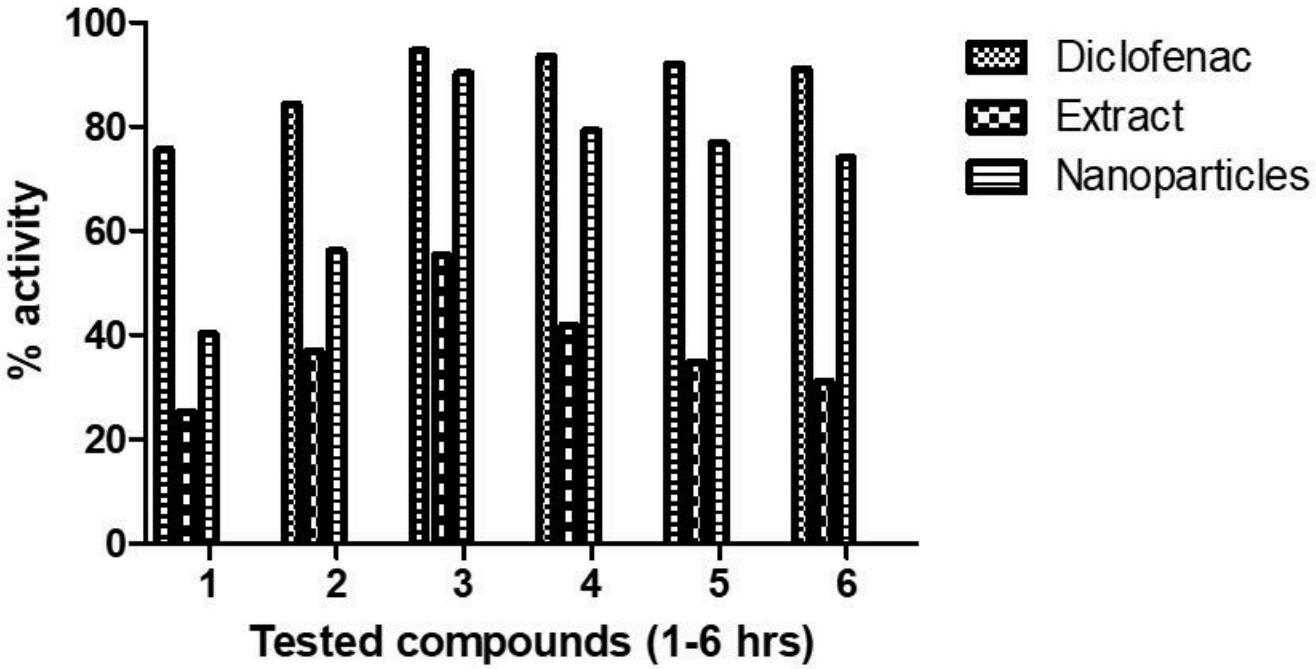

Figure 7

Anti-inflammatory activity of Iron NPs.